FT-IR Imaging of Polymer Dissolution by Solvent Mixtures. 1. Solvents

Travis Ribar, Rohit Bhargava,† and Jack L. Koenig*

Department of Macromolecular Science, Case Western Reserve University, Cleveland, Ohio 44106

Received May 17, 2000; Revised Manuscript Received August 18, 2000

ABSTRACT: The dissolution of poly(α-methylstyrene) (PAMS) by a binary solvent mixture containing systematically varied amounts of methyl isobutyl ketone (MIBK) in deuterated cyclohexane was studied using FT-IR imaging. From each sequential image in a timed sequence, spatially resolved spectral data were gathered and absorbance profiles for the field of view were obtained. This allowed the study of solvent penetration and quantitative analysis of the dissolution process from concentration profiles. The dissolution of the polymer was found to vary linearly with time for ∼150 μm dissolved layer. The dissolution rate was found to increase linearly with MIBK concentration. In each solvent mixture, diffusion profiles were characteristic of case II diffusion. No solvent component segregation was seen. It is demonstrated that FT-IR imaging is a viable tool to characterize the dissolution of polymers by multicomponent solvents.

Introduction

The diffusion of low molecular weight species into polymers is a research field with widespread practical applications. Penetrant diffusion studies are useful in areas ranging from time-release drugs,[1−3] paint formation, membrane transport, and liquid crystal composites to lithographic techniques used to manufacture microchips. Very often the process is complicated by the presence of two or more constituents and complex geometrical shapes combined with convective effects. The first steps toward understanding such a process are diffusion experiments with no convection effects. Such model experiments would yield information about the type of diffusion, dissolution rate, and concentration dependence of the process as a function of experimental conditions.

While there is good understanding of the diffusion of a single solvent into a polymer,[4] the (inter) diffusion of multicomponent systems is not that well understood. The study of polymer dissolution by mixed solvents is directly applicable to many fields, e.g., current lithographic techniques that often call for polymer dissolution by solvent mixtures. Since the quality of the resulting product is partly dependent on the solvent composition, it is important to know how solvent mixtures dissolve a bulk polymer. Such studies are motivated by financial process considerations as well. An expensive, good solvent for a polymer might be diluted with a cheaper, poorer solvent. The loss in production time would be more than offset by savings in solvent costs. Clearly, to yield lowest cost production, determination of dissolution behavior based on solvent composition would need to be understood. Hence, studies of multicomponent solvent dissolution of a polymer are not only scientifically relevant but are also of commercial importance.

Examining polymer dissolution by mixed solvents is made difficult by its requirements. In many cases, the dissolution of polymers in mixed solvents has been characterized by observing the effect of the composition of solvent mixture on the dissolution rate of the polymer and not the behavior of each individual component in the mixture during dissolution.[5,6] It is unknown in these experiments whether all components are diffusing into the polymer at the same rate, whether there is exclusion of one solvent, and whether solvent concentration at the polymer−solvent interface is different than in the bulk solvent solution. The solvent diffusion rate compared to the rate of polymer relaxation is the primary factor affecting the type of diffusion process seen.[7] The amount of solvent absorbed by a polymer as a function of time, M_t, can be used to characterize the diffusion process, i.e., for

$$M_t = kt^n \tag{1}$$

the exponent n characterizes the diffusional behavior. An exponent of 0.5 likely implies Fickian (case I) diffusion while an exponent close to 1 likely implies non-Fickian (case II) diffusion. An exponent between 0.5 and 1.0 signifies anomalous diffusion. Case II and anomalous diffusion are usually observed for polymer whose glass transition temperature is higher than the experimental temperature. In general, case II behavior is observed for solvents with high activities.[8] Case II diffusion is characterized by a rapid increase in solvent concentration in the polymer region with a sharp penetration front which advances at a constant rate. There is also an induction time for the Fickian concentration profile that precedes the solvent penetration front. It has been reported that the composition of the solvent may also lead to crossover from one type of diffusion behavior to another.[9] Thus, analysis of solvent mixture diffusion must take into account the diffusion profiles for each solvent.

A number of experimental techniques have been employed for analyzing model diffusion studies. Traditional gravimetric ("blot-and-weigh") methods[10] are a form of physical analysis that determines mass uptake as a function of time. Bulk chemical analysis techniques such as NMR,[11] polar ellipsometry,[12,13] FT-IR spectroscopy,[14−16] and ATR spectroscopy[14,17,18] yield chemical information. Microscopy,[19] refractive index measurements,[20] radiation detection due labeling,[21] and Rutherford backscattering spectroscopy[22] yield high spatial resolution images based on optical properties, but

† Current address: Laboratory of Chemical Physics, NIDDK, National Institutes of Health, Bethesda, MD 20892.

* To whom correspondence should be addressed.

10.1021/ma000851r CCC: $19.00
Published on Web 10/21/2000

usually do not contain specific chemical information. Detection based on labeling techniques such a fluorescence labeling[23,24] perturbs the system and may not be routine to carry out. These methods of analysis are incapable of yielding both the spatial and chemical data that would make a dissolution experiment fast and easy to conduct. Imaging techniques are a step in that direction. Magnetic resonance imaging (MRI) has been used to characterize polymer dissolution.[9,25,26] However, the spatial resolution of these experiments is close to a fraction of a millimeter, experimental times are long, and fast diffusion phenomena may not be examinable. FT-IR microspectroscopy offers an improvement in spatial resolution over NMR imaging and yields images that have spatially resolved data on the order of microns.

Until recently, FT-IR microspectroscopy was carried out using apertures to limit the spatial area examined and then obtaining chemical information (an IR spectrum) for the area using a single element detector. The apertures were then used to sequentially limit the area examined and characterize the diffusion region. This technique was most frequently applied to "static" diffusion regions, e.g., polymer−polymer interdiffusion or slow diffusion processes. Microtoming, which was a laborious process, was avoided in many cases by using the contact method.[27] However, the profiles had to be made static by reducing the temperature or polymerizing one component to "freeze-in" the profile or examine slow diffusion processes. For real-time experiments, linear velocity of the penetrant examinable was limited to 10−20 μm/h. Recently, the coupling of a focal plane array detector to a spectrometer[28] has given us the capability to image large fields of a view in a single collection step. A field of view spanning hundreds of microns may be imaged in less than 5 min with spatial resolutions approaching the IR diffraction limit. Compared to the single detector microspectroscopic technique, comparable data are obtained much faster and at a higher spatial resolution.[29] This technique has been applied to a small number of studies of multicomponent polymer systems ranging from semicrystalline polymers[30] to polymer−liquid crystal composites[31,32] and diffusion processes.[33,34] The dissolution of a polymer by a solvent[35] with linear velocities as large as 5 μm/s is monitorable[36] with high signal-to-noise ratio data sets.[37] This is adequate for most polymer−solvent diffusion studies.

This paper seeks to report the dissolution of a low molecular weight polymer by a binary solvent mixture. Entanglement effects do not complicate the dissolution process, and both diffusants are solvents for the polymer. Hence, dissolution is expected to be fast. The effectiveness of FT-IR imaging as a tool to characterize this process is examined. The type of diffusion process, segregation of components, and obtaining the dissolution rate are primary aims of the paper.

Experimental Section

PAMS (M_n ~790, T_g ~ 49° C) was used as received[38] in this experiment. Weight ratios of as-received solvents (deuterated cyclohexane[38] (99.6% deuterated) and methyl isobutyl ketone (MIBK)) were used. Experiments were conducted using the contact method.[27] To prepare a thin layer of polymer sandwiched between two salt plates, a small granule of solid polymer was placed on 2 mm thick CaF_2 substrates and was heated on a hot stage to 150 °C. A substrate was then placed on top of the polymer granule, and the two plates were clamped together. The sample was then placed in an oven at 150 °C for 2 h, after which it was allowed to cool in ambient air to room temperature. The clamps were removed to yield a polymer film partially occupying space between the two plates. Solvent was introduced from the empty end after the sample interface was positioned in the spectrometer. The solvent entered the space between the substrates due to capillary action and came into contact with the polymer. Images were sequentially acquired during the time it took the solvent mixture to completely dissolve the polymer from the field of view. Solvent solution was added as necessary.

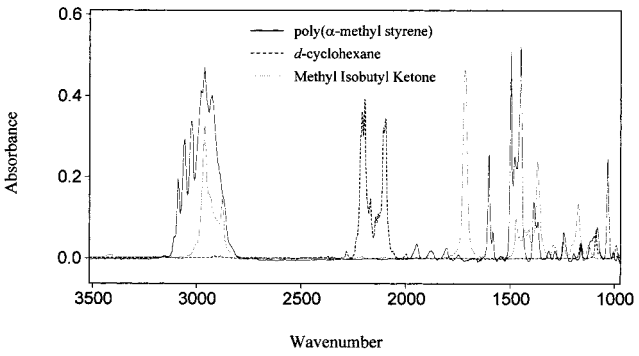

Figure 1. Spectra and peaks used to obtain concentration profiles for the polymer and solvents.

Infrared images were acquired using the Bio-Rad Stingray imaging spectrometer. The Stingray is comprised of the FTS 6000 step-scan interferometer bench coupled to a microscope accessory, UMA-500.[39] The imaging detector is a Santa Barbara Focal Plane FPA of 64 × 64 mercury cadmium telluride (MCT) elements imaging an average spatial area of 500 μm × 500 μm in a single experiment. A long pass filter to eliminate unwanted wavelengths and prevent Fourier fold-over perturbations is inserted into the beam path. An 8 cm^{-1} nominal spectral resolution and an undersampling ratio (UDR) of 4 were used for the study. A mirror stepping rate of 5 Hz was used to give a total scanning time of about a 210 s. The number of camera frames (frame rate = 316 Hz; integration time = 0.0938 ms) averaged during each spectrometer step was 20. Image processing and data extraction were carried out using the hyperspectral imaging software package Environment for Visualizing Images (ENVI).[40] Lower noise absorbance profiles were extracted from each image by averaging the spectral data from a 40 μm wide cross section of the image.

Results and Discussion

Absorbance and Concentration Profiles. The spatial distribution of a component in the field of view can be monitored using its characteristic IR absorbance peak. Absorbance spectra for the neat solvent mixture components and polymer can be seen in Figure 1. The peak at 1600 cm^{-1}, representing the ring quadrant stretching mode, was used to characterize the polymer. Peaks at 1730 cm^{-1} (C═O stretching vibration) for MIBK and 2100 cm^{-1} (CD stretching) for *d*-cyclohexane were used to monitor solvent concentration. From each image data cube collected during the experiment, these specific frequencies may be used to yield absorbance images. Images obtained by plotting the characteristic absorbance frequency for each component may be seen in Figure 2a−c. The images are obtained by thresholding data based on the color bar shown in the image. Absorbance profiles for the polymer and each of the solvents in the solvent solution can be extracted perpendicular to the film edge. Figure 2d−f shows a typical group of absorbance profiles corresponding to the images a−c, respectively. It can be seen that one image data cube collection yields spatially resolved absorbance data

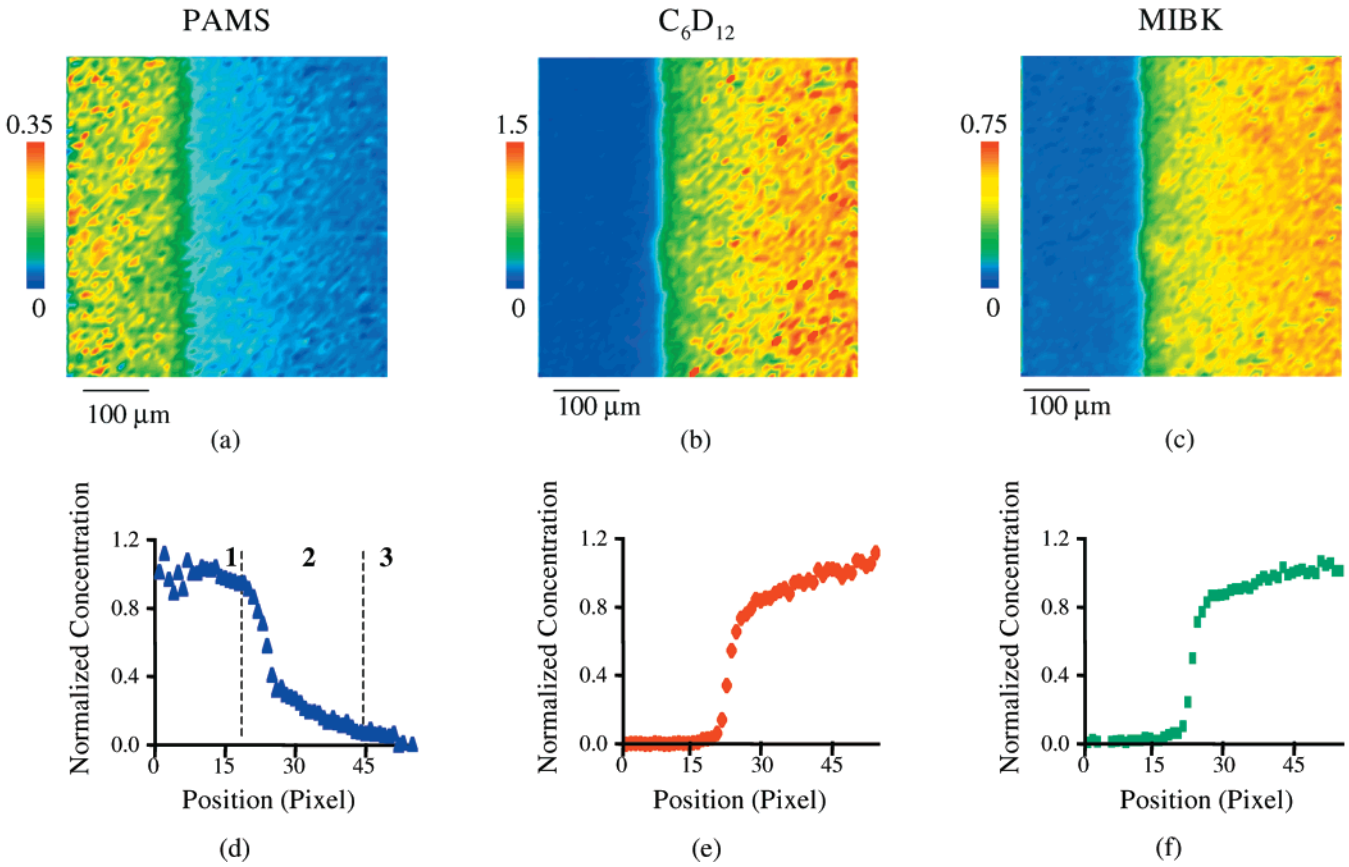

Figure 2. PAMS, C_6D_{12}, and MIBK absorbance images and profiles taken from dissolution in an 85:15 C_6D_{12}:MIBK solvent solution. The three distinct regions seen in the absorbance profile for the polymer are (1) bulk polymer region, no solvent; (2) dissolved polymer layer; and (3) neat solvent mixture, no polymer.

for all components involved. This chemical specificity combined with high spatial specificity is uniquely achieved through FT-IR imaging in a short time.

An examination of the absorbance profiles shows that each profile may contain up to three different regions reflecting the dissolution process. The three regions may be seen in Figure 2a,d. The region of high absorbance (region 1 in the profile pictured) reflects the bulk polymer, while the region of low absorbance (region 3) reflects an area in which there is no polymer. A middle region forms during the experiment as time progresses. This region of intermediate absorbance (region 2) is due to polymer chains dissolved from the bulk polymer. The region of dissolved polymer chains is unique to the dissolution process. It has been shown that there are optical distortions at a sharp refractive index interface that lead to baseline offsets[31] and small spectral distortions. Before discussing the region between the bulk polymer and bulk solvent, it needs to be determined that optical effects that result from the high contrast at the polymer−solvent interface do not significantly affect the absorbance profiles.

A typical absorbance profile derived from a single row across the interface can be seen in Figure 3. This profile is for an image with a polymer−air interface before the introduction of solvent. At this point, the refractive index mismatch is at a maximum in our system. The profile shows a sharp decrease in absorbance between the polymer bulk and air regions of the sample. Ideally, the normalized absorbance should drop to zero from 1. However, the edge may not correspond exactly with pixel edges, the polymer sample may not have a sharp thickness decrease, and there is diffraction at the edges. There are also small effects associated with focusing at a certain wavelength and imaging at another. Hence, the drop in bulk values over 2−3 pixels is reasonable, and errors associated with all these factors affect no more than 3−4 pixels. The refractive index and diffraction effects are lower with the introduction of a solvent (closer refractive index to the polymer than air) and with the establishment of a diffusion profile (destroying the sharp interface). Hence, the effects of refractive index mismatches can be discounted from any physical effects observed in concentration profiles, especially at later times. Therefore, we can conclude that region 2 in Figure 2d is a true reflection of dissolved polymer chain concentration at the polymer−solvent interface and not due to optical effects.

Because of the lack of convection in the experimental setup, this polymer has not been carried away from the polymer−solvent interface. Such studies are of importance to study the dissolution of polymers without convection. They are also the first steps toward modeling the dissolution−convection process (vide infra). The complete dissolution process can be imaged as a function of time by collecting images of the same area sequentially. A typical case is shown in Figure 4. Dissolution of the polymer by the solvent mixture can be seen as a function of time. The concentration of the polymer increases in the regions that contained mainly solvent at an earlier time. The solvent ingress into the polymer can also be clearly seen.

Absorbance profiles for each component can be extracted at different times and are shown with their respective images in Figure 5 for another case. The profiles reflect the intensity of an IR peak as a function

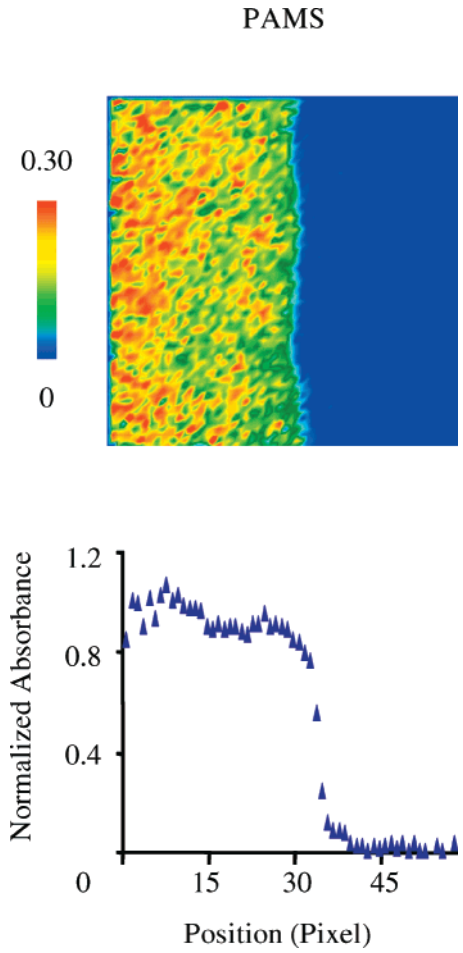

Figure 3. Absorbance image of PAMS and the corresponding absorbance profile for PAMS in the image. The image is thresholded to the values on the color bar to the left.

of position. Beer's law states that the absorbance of a given band is proportional to the absorptivity of that band, the thickness of the sample, and the concentration of the sample,

$$A = abc \tag{2}$$

The sample thickness in this experiment and optical parameters for any given peak are constant. Hence, the absorbance of a band is directly related to its concentration in the sample, and absorbance profiles are equivalent to concentration profiles for each component. Since the pure components and the diffusion region can be observed in the same image, a convenient normalizing absorbance is obtainable. Therefore, the normalized absorbance profiles extracted from each spectral image are normalized concentration profiles as well and the terms "concentration profile" and "absorbance profile" are used synonymously in this paper.

Polymer Dissolution and Solvent Diffusion. Typical concentration profiles for the polymer as a function of time may be seen in Figure 6a. The rate of dissolution can be determined by plotting the position of the polymer−solvent interface as a function of time. The local slope of the fitted curve is the velocity of the interface at that time (Figure 6b). The dissolution rate is then, simply, a product of this solvent ingress velocity multiplied by the perpendicular area exposed to the solvent. It is noteworthy that the velocity of the dissolving front is a linear function of time in this case. Examining the velocity of the diffusion front for the slowest dissolving case (Figure 6c), the rate is seen to decrease slightly with time at large times. As a first approximation, the rate of dissolution is approximately constant over time. However, a linear fit over the whole region (dotted line) is certainly a poorer fit compared to an exponential decay curve (solid line). A dashed line fitting the early part of the dissolution process shows a

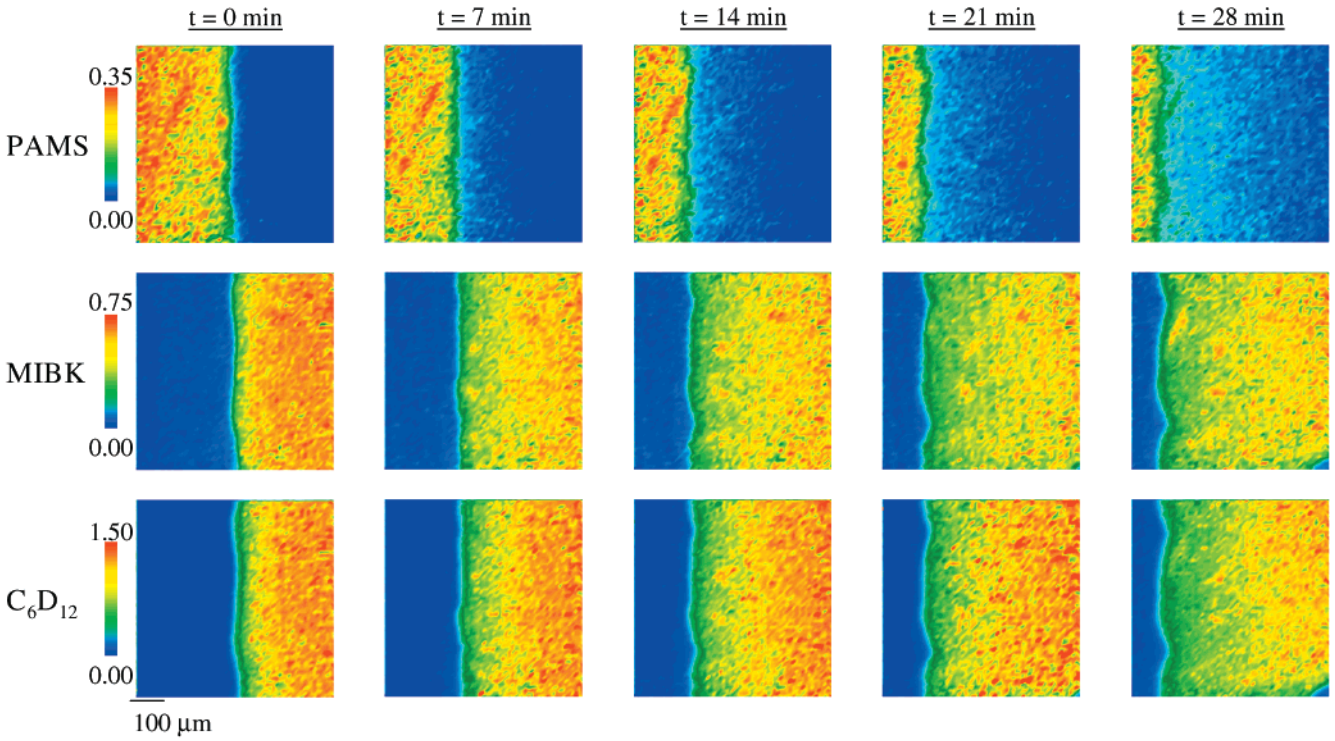

Figure 4. Spectral images showing the concentration of PAMS, MIBK, and C_6D_{12} during the dissolution of PAMS in an 85/15 C_6D_{12}/MIBK solvent solution.

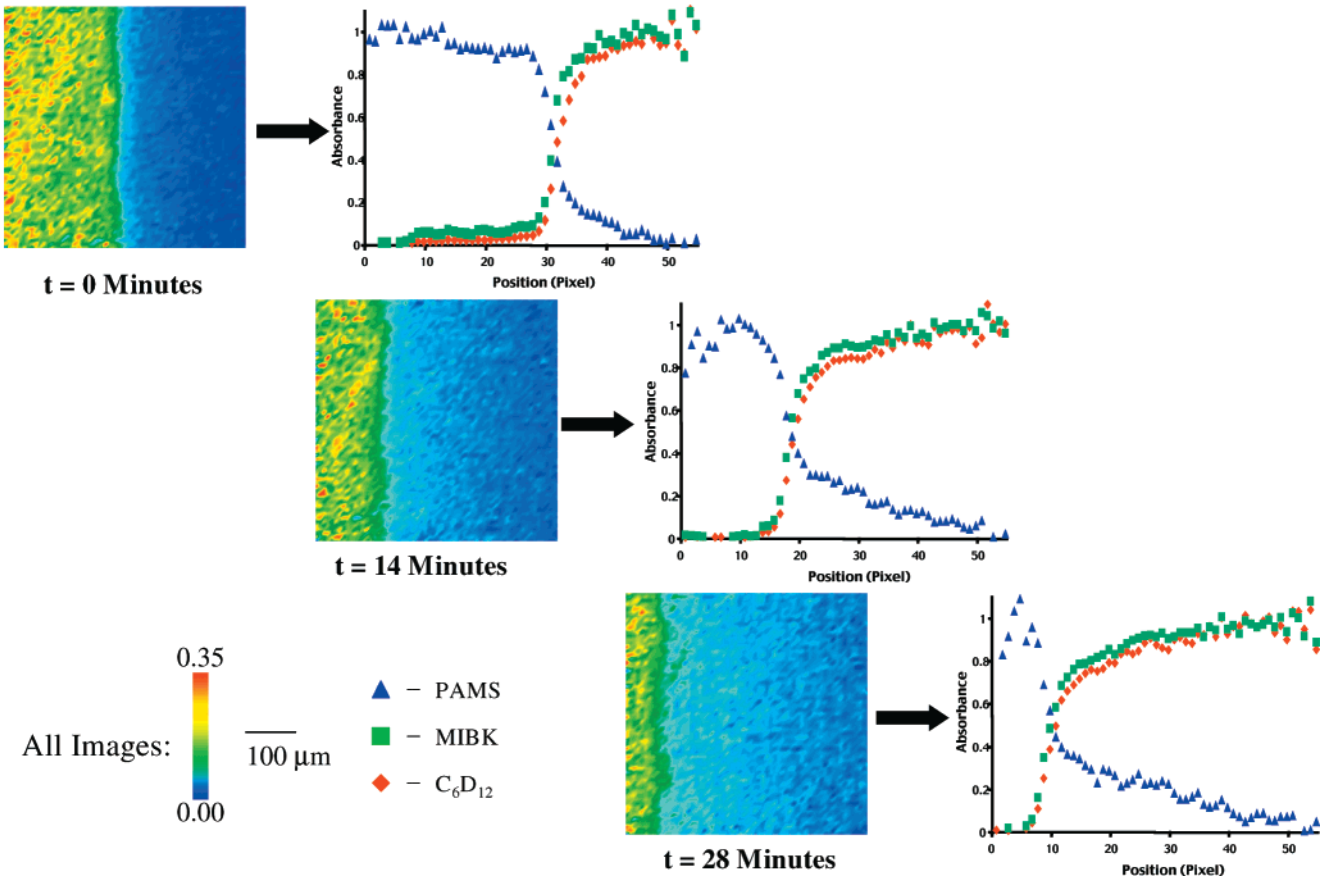

Figure 5. Images reflecting the absorbance of PAMS during dissolution in an 80/20 C_6D_{12}/MIBK solvent solution. Absorbance profiles reflect the absorbance of PAMS, C_6D_{12}, and MIBK.

good fit for the data, but deviations are seen for longer times. This is probably due to the dissolved chains remaining at the polymer−solvent interface. Dissolved chains cause an increase in the viscosity of the solvent at the interface that acts to decrease further dissolution of the PAMS. As the width of the dissolved polymer region increases with time, the dissolution process is hindered. This leads to a slight decrease in the rate of dissolution. However, it may be concluded that this decrease is minor for a boundary layer spanning over a hundred microns. This is probably due to the nature of the solvents and the low molecular weight used. This finding has implications in the boundary layer modeling of the dissolution process incorporating convection for such systems. The dissolution rate would be affected by convective effects only in cases where the dissolved layer is greater than a few hundred microns. Hence, maintaining a continuous convective flow is not required for such a system and a single flushing after required dissolution is achieved would be sufficient. A series of experiments, such as conducted in this paper, would yield system specific information useful for modeling in a short time.

Linear fits to the dissolution rates for solvents of different compositions can be seen in Figure 7a. The dissolution rate of the polymer based on the dissolving front is plotted as a function of *d*-cyclohexane content of the solvent mixture. The dissolution profiles again show a reasonable linear fit. Increasing slopes with increasing MIBK content show a general trend toward faster dissolution. This trend may be seen in Figure 7b. The penetration rates derived from this analysis are shown in Table 1. The error calculated can be seen to

Table 1. Penetration Velocity as a Function of Solvent Composition and Corresponding Fit for a Linear Regression Analysis; Error Values Are the Standard Deviation from Fit Values

solvent composition C_6D_{12}:MIBK	penetration velocity (μm/min)	error	R^2
100:0	4.07	0.28	0.9689
95:5	4.02	0.24	0.9977
90:10	5.45	0.44	0.9937
85:15	6.88	0.34	0.9897
80:20	7.85	0.55	0.9805
70:30	10.24	0.81	0.9814

be 5−8% in most cases. The dissolution rate varies linearly with the concentration of *d*-cyclohexane in the mixture. On the basis of the dissolution rates of the neat solvents, the rate for a binary mixture may be predicted using a simple composition weighting function,

$$R_{mix} = R_{MIBK}(\phi_{MIBK}) + R_{d-cyclohex}(1 - \phi_{MIBK}) \quad (3)$$

This prediction is compared to the experimentally obtained values of the dissolution rate in Table 2. In general, the trend predicted by the model above is followed. However, the fit is better for larger MIBK concentrations. The error in prediction for the lower concentrations increases with decreasing MIBK concentration. This appears to indicate that the diffusion process is also influenced by a nonlinear composition term. If another term is added to (3) and the equation modified to

$$R_{mix} = R_{MIBK}(\phi_{MIBK}) + R_{d-cyclohex}(1 - \phi_{MIBK}) + k(\phi_{MIBK})(1 - \phi_{MIBK}) \quad (4)$$

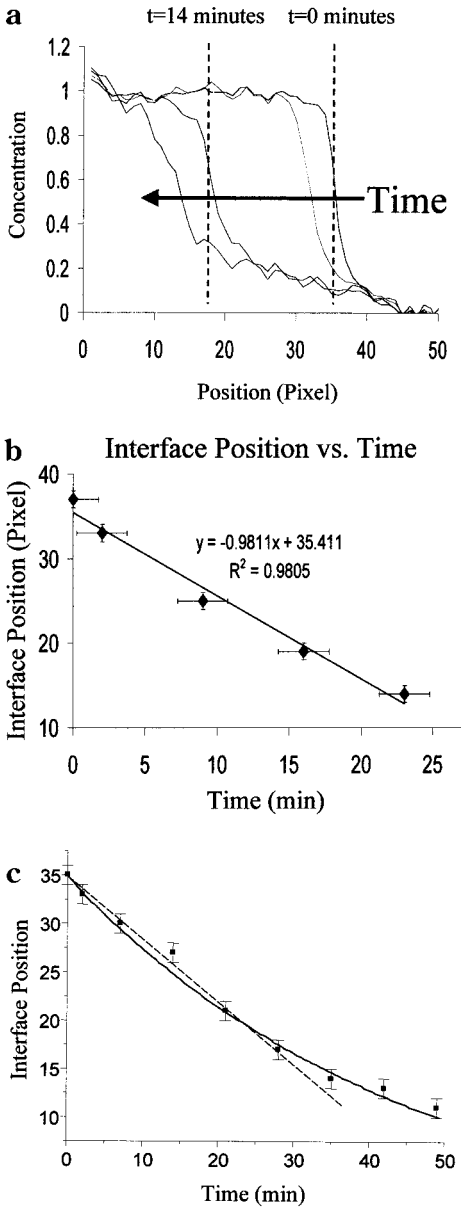

Figure 6. (a) PAMS absorbance profiles from dissolution in an 80/20 C_6D_{12}/MIBK solvent solution. (b) A plot of the interface position versus time allows for the derivation of the rate of dissolution. (c) Dissolution rate as a function of time for the dissolution of PAMS by *d*-cyclohexane. The line with the greater slope is fit to the first 100 μm. The second line is fit to the entire data set.

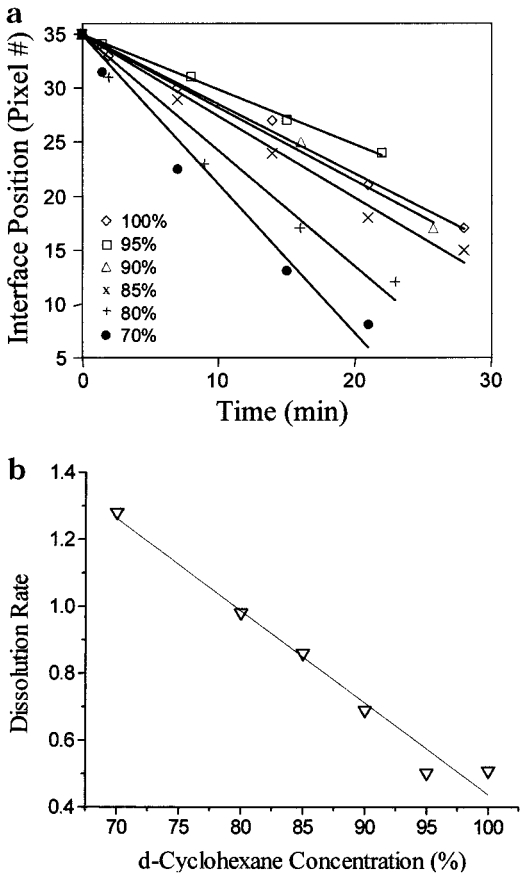

Figure 7. Absorbance profiles of dissolution in three solvent mixtures and the associated graph showing the dissolution rate of each. From the dissolution rate of each solvent mixture, the linear relationship between dissolution rate and solvent composition may be seen.

Table 2. Comparison of Predicted to Experimentally Obtained Dissolution Rates for Poly(α-methylstyrene) Dissolved by an MIBK/*d*-Cyclohexane Mixture as a Function of *d*-Cyclohexane Content; MIBK Dissolution Rates Were Obtained by Monitoring the Refractive Index Front on the Bright-Field IR Image

wt % *d*-cyclohexane	linear model rate (μm/min)	obsd rate (μm/min)	fract error	nonlinear model (μm/min)	fract error
100	4.07	4.07	0.00	4.07	0.00
95	5.11	4.02	0.21	4.95	0.19
90	6.16	5.45	0.11	5.86	0.07
85	7.21	6.88	0.05	6.82	−0.01
80	8.26	7.85	0.05	7.81	0.00
70	10.35	10.24	0.01	9.91	−0.03

the cross-correlation term accounts for differences seen between the rates to a much greater extent. Fitting the parameter *k* to a value yielding a minimum in deviation from observed values, we see that the error is indeed lower for this nonlinear model. However, the deviation for 5% MIBK solution is still very large and unexplained. A possible reason could be the segregation of solvents during the experiment. The increased activity of the high MIBK concentration may be a result of the high dissolution rate MIBK. This solvent may act to first dissolve the polymer at the interface and, hence, enhance dissolution rates for the mixture. This issue is examined by characterization of the individual solvent profiles.

The diffusion of the solvent mixture may also be characterized by the diffusion profiles of each component (Figure 8a,b). Typical diffusion profiles (in this case, an 80:20 mixture) may be seen as a function of time. The profiles are characteristic of case II profiles with an initial Fickian induction profile followed by a sharp penetrating front at later times. The front can be seen below the dotted line and the solvent concentration is constant in the region following the front. A plot of the penetration front position as a function of time (Figure 8c) reveals a linear dependence. Thus, both solvents meet the criteria for case II behavior. As opposed to some studies which report a crossover from case II to case I diffusional behavior,[9] the system exhibited case II behavior for all composition ranges at the experimental temperature.

Solvent Composition. From Figure 8c, it can also be seen that the interfaces of both the MIBK and the *d*-cyclohexane are located at the same point. This

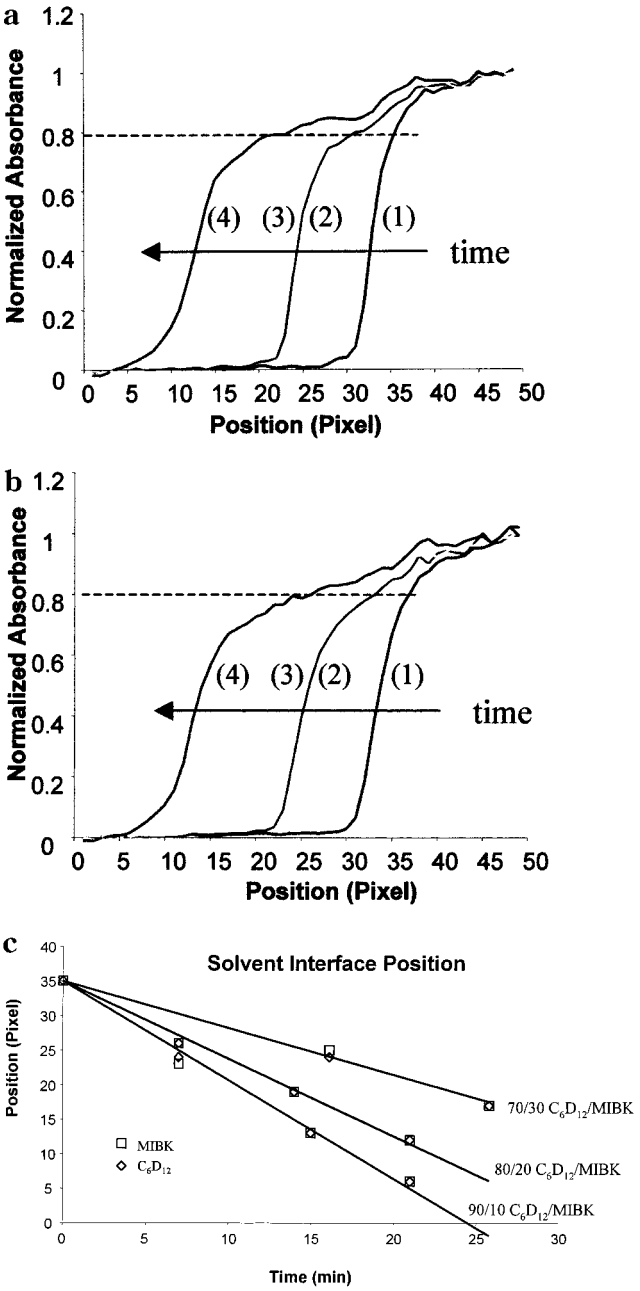

Figure 8. Absorbance profiles of (a) MIBK and (b) C_6D_{12} taken from PAMS dissolution by an 80/20 C_6D_{12}/MIBK solvent mixture. Profiles were taken from images acquired at 0, 7, 14, and 21 min after solvent−polymer contact. (c) The interface position of each component of the solvent over time for three solvent mixtures.

implies that the MIBK and the *d*-cyclohexane were diffusing into the PAMS at the same rate. This is interesting because neat MIBK and neat *d*-cyclohexane diffuse into PAMS at widely different rates. For binary solvents, one solvent may have a higher molecular weight or be a better solvent than the other. Hence, a solvent segregation may be expected. In this case, the molecular weights of the two solvents are very close (96 for C_6D_{12} compared to 101 for MIBK). Hence, solubility parameters are expected to determine any segregation of the mixture components. The solubility parameters[41] for the solvents and the polymer are shown in Table 3. Consistent with the neat solvent dissolution rates, MIBK is a somewhat better solvent than *d*-cyclohexane for PAMS. Hence, it was a possibility that MIBK

Table 3. Solubility Parameters for the Polymer and Solvents

material	solubility parameter, δ (MPa$^{1/2}$)	$(\delta_{polymer} - \delta_{solvent})^2$
polymer (PAMS)	19.3	0.0
d-cyclohexane	16.8	6.4
MIBK	17.2	4.5

diffusion through the dissolved polymer layer is faster than the *d*-cyclohexane. This would create a mixture concentration at the interface that had a higher concentration of MIBK than the solution that was being added. To determine whether this was the case, the ratio of the absorbance of the two solvent-specific IR peaks was taken across the same cross section as the concentration profiles. Referring back to Beer's law, the ratio of the absorbance of two bands may be written as

$$\frac{A_1}{A_2} = \frac{a_1 b c_1}{a_2 b c_2} \tag{5}$$

where A_1, a_1, b, and c_1 are absorbance, absorptivity, cell thickness, and concentration for the first solvent and A_2, a_2, b_2, and c_2 are for the other solvent. Since a_1/a_2 is a constant and because the thickness of the sample is constant, this equation may be reduced to

$$\frac{A_1}{A_2} = k\left(\frac{c_1}{c_2}\right) \tag{6}$$

where k is a constant. Therefore, the ratio of the absorbance of the two solvent peaks reflects the composition of the solvent solution. Figure 9 plots the value of this ratio and the corresponding PAMS concentration profile for a typical case. As there is no change in the value of the ratio, as evidenced by the horizontal line on the graph, it can be concluded that the solvent solution composition remains constant throughout the solvent solution. If indeed there is segregation, it is on a scale smaller than the resolution limit of the imaging spectrometer. This result was found for all times in all solvent mixtures examined in this paper. This simple analysis serves to illustrate a very powerful application of the FT-IR imaging technique that is possible with no other technique in such a simple manner.

Conclusions

FT-IR imaging was successfully applied to examine the dissolution of a polymer by a binary solvent mixture in real time. Spatially resolved spectral data from a multicomponent diffusion system allowed for the simultaneous characterization of all components within that system. From the images collected, the nature of the diffusion process, concentration profiles, dissolution rates, and solvent composition were determined. The dissolution rates for the neat polymer and the mixtures were obtained from concentration profiles. Polymer dissolution rates were found to be approximately linear with time for dissolved layers as large as 150 μm. It was hypothesized that the increase in viscosity that the layer produced created a slight decrease in the rate of diffusion at later times. A linear relationship between the rate of dissolution and the concentration of MIBK in the solvent mixture was also established. From the dissolution behavior seen in these model experiments, important clues to process optimization for polymer dissolution are obtained. Solvent diffusion into the

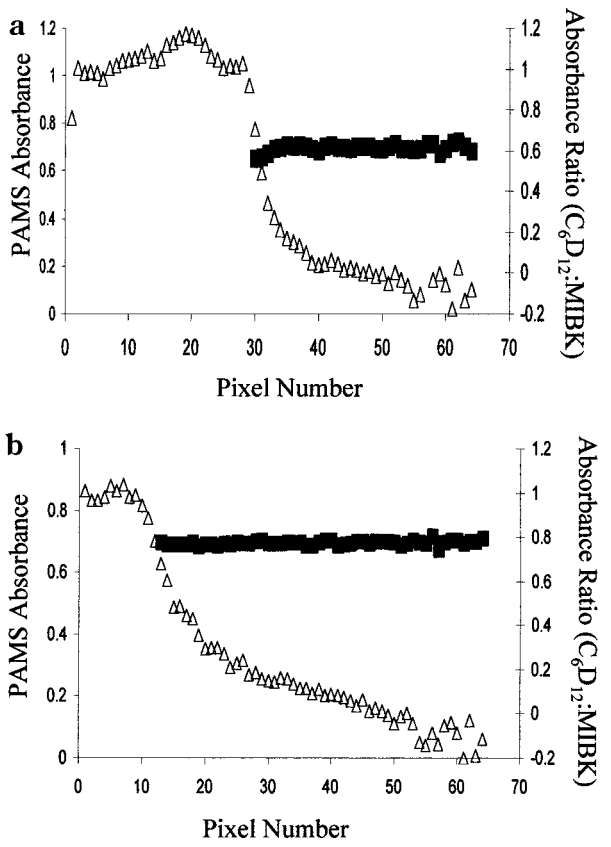

Figure 9. (a) Absorbance profile for the polymer and a profile of the ratio of solvent mixture components' absorbance for a 70:30 *d*-cyclohexane:MIBK mixture at the start of the experiment and a similar plot (b) for a time corresponding to 15 min of polymer dissolution.

polymer was characterized as case II type of diffusion. The system imaged here reflects a polymer in contact with two solvents, though MIBK diffuses into PAMS faster than *d*-cyclohexane. The composition of the solvent that reached the bulk polymer was the same as the starting composition in all cases. It is demonstrated that complex diffusion processes involving many components can be readily analyzed using FT-IR imaging.

Acknowledgment. Funding from the National Science Foundation Advanced Liquid Crystal Optical Materials (ALCOM) via Grant DMR89-20147 is acknowledged.

References and Notes

(1) Heller, J.; Baker, R. W.; Gale, R. M.; Rodin, J. O. *J. Appl. Polym. Sci.* **1978**, *22*, 1991.
(2) Korsmeyer, R. W.; Lustig, S. R.; Peppas, N. A. *J. Polym. Sci., Polym. Phys.* **1986**, *24*, 395.
(3) Lee, P. I. *J. Controlled Release* **1985**, *2*, 277.
(4) Masaro, L.; Zhu, X. X. *Prog. Polym. Sci.* **1999**, *24*, 731.
(5) Papanu, J. S.; Hess, D. W.; Soane, D. S.; Bell, A. T. *J. Electrochem Soc.* **1989**, *136* (10), 3077.
(6) Manjkow, J.; Papanu, J. S.; Soong, D. S.; Hess, D. W.; Bell, A. T. *J. Appl. Phys.* **1987**, *62* (2), 682.
(7) Alfrey, T., Jr.; Gurnee E. F.; Lloyd, W. G. *J. Polym. Sci., Part C* **1966**, *12*, 249.
(8) Weisenberger, L. A.; Koenig, J. L. *Macromolecules* **1990**, *23*, 2445.
(9) Grinsted R. A.; Clark, L.; Koenig, J. L. *Macromolecules* **1992**, *25*, 1235.
(10) Mandelkern, L.; Long, F. A. *J. Polym. Sci.* **1951**, *6*, 457.
(11) Bastow, T. J.; Hodge, R. M.; Hill, A. J. *J. Membr. Sci.* **1997**, *131*, 207.
(12) Papanu, J. S.; Hess, D. W.; Bell, A. T.; Soane, D. S. *J. Electrochem. Soc.* **1989**, *136* (4), 1195.
(13) Papanu, J. S.; Hess, D. W.; Soane, D. S.; Bell, A. T. *J. Appl. Polym. Sci.* **1990**, *39*, 803.
(14) Schlotter, N. E.; Furlan, P. Y. *Vib. Spectrosc.* **1992**, *3*, 147.
(15) Van Alsten, J. G.; Lustig, S. R. *Macromolecules* **1992**, *25*, 5069.
(16) Jabbari, E.; Peppas, N. A. *Macromolecules* **1993**, *26*, 2175.
(17) Fieldson, G. T.; Barbari, T. A. *Polymer* **1993**, *34*, 1146.
(18) Fieldson, G. T.; Barbari, T. A. *AIChE J.* **1995**, *41*, 795.
(19) Thomas, N. L.; Windle, A. H. *Polymer* **1977**, *18*, 1195.
(20) Crank, J.; Robinson, C. *Proc. R. Soc. London A* **1950**, *204*, 339.
(21) Bueche, F.; Cashin, W. M.; Debye, P. V. *J. Chem. Phys.* **1952**, *20*, 1956.
(22) Mills, P. J.; Palmstrom, C. J.; Kramer, E. J. *J. Mater. Sci.* **1986**, *21*, 1479.
(23) O'Niel, G. A.; Torkelson, J. M. *Macromolecules* **1997**, *30*, 5560.
(24) Wisnudel, M. B.; Torkelson, J. M. *Macromolecules* **1996**, *29*, 6193.
(25) Weisenberger, L. A.; Koenig, J. L. *Appl. Spectrosc.* **1989**, *43* (7), 1117.
(26) Grinsted R. A.; Clark, L.; Koenig, J. L. *Macromolecules* **1992**, *25*, 1235.
(27) Challa S. R.; Wang, S.-Q.; Koenig, J. L. *Appl. Spectrosc.* **1996**, *50* (11), 1339.
(28) Lewis, E. N.; Treado, P. J.; Reeder, R. C.; Story, G. M.; Dowrey, A. E.; Marcott, C.; Levin, I. W. *Anal. Chem.* **1995**, *67*, 3377.
(29) Bhargava, R.; Wall, B. G.; Koenig, J. L. *Appl. Spectrosc.*, in press.
(30) Snively, C. M.; Koenig, J. L. *J. Polym. Sci., Part B* **1999**, *37*, 2353.
(31) Bhargava, R.; Wang, S.-Q.; Koenig, J. L. *Appl. Spectrosc.* **1998**, *52*, 323.
(32) Bhargava, R.; Wang, S.-Q.; Koenig, J. L. *Macromolecules* **1999**, *32*, 2748.
(33) Snively, C. M.; Koenig, J. L. *Macromolecules* **1998**, *31*, 3753.
(34) Snively, C. M.; Koenig, J. L. *J. Polym. Sci., Part B* **1999**, *37*, 2261.
(35) Koenig, J. L.; Snively, C. M. *Spectroscopy* **1998**, *13*, 22.
(36) Bhargava, R.; Ribar, T.; Koenig, J. L. *Appl. Spectrosc.* **1999**, *53* (11), 1313.
(37) Bhargava, R.; Wang, S.-Q.; Koenig, J. L. *Appl. Spectrosc.*, in press.
(38) Aldrich Chemical Co., Milwaukee, WI.
(39) Bio-Rad, Digilab Laboratories, Cambridge, MA.
(40) RSI, 2995 Wilderness Drive, Boulder, CO 80301.
(41) Grulke, E. A. Solubility Parameter Values. In *Polymer Handbook*, 3rd ed.; Brandrup, J., Immergut, E. H., Grulke, E. A., Eds.; Wiley: New York, 1989; Vol, II, p 675.

MA000851R